Journal Pre-proofs

Use of an optofluidic microreactor and Cu nanoparticles synthesized in ionic liquid and embedded in TiO_2 for an efficient photoreduction of CO_2 to methanol

Jonathan Albo, Muhammad I. Qadir, Mario Samperi, Jesum Alves Fernandes, Imanol de Pedro, Jairton Dupont

PII: S1385-8947(20)32771-6
DOI: https://doi.org/10.1016/j.cej.2020.126643
Reference: CEJ 126643

To appear in: *Chemical Engineering Journal*

Received Date: 14 April 2020
Revised Date: 7 August 2020
Accepted Date: 8 August 2020

Please cite this article as: J. Albo, M.I. Qadir, M. Samperi, J. Alves Fernandes, I. de Pedro, J. Dupont, Use of an optofluidic microreactor and Cu nanoparticles synthesized in ionic liquid and embedded in TiO_2 for an efficient photoreduction of CO_2 to methanol, *Chemical Engineering Journal* (2020), doi: https://doi.org/10.1016/j.cej.2020.126643

Use of an optofluidic microreactor and Cu nanoparticles synthesized in ionic liquid and embedded in TiO_2 for an efficient photoreduction of CO_2 to methanol

Jonathan Albo[a,], Muhammad I. Qadir[b,c], Mario Samperi[d,e], Jesum Alves Fernandes[e], Imanol de Pedro[f], Jairton Dupont[b]*

[a]Department of Chemical & Biomolecular Engineering, University of Cantabria (UC), Avda. Los Castros s/n, 39005 Santander, Spain

[b]Institute of Chemistry–UFRGS, Av. Bento Gonçalves, 9500, Porto Alegre, 91501-970, RS, Brazil

[c]Department of Nanocatalysis, J. Heyrovský Institute of Physical Chemistry, Dolejškova 2155/3, 18223 Prague 8, Czech Republic

[d]School of Pharmacy, University of Nottingham, University Park, NG7 2RD, United Kingdom

[e]School of Chemistry, University of Nottingham, NG7 2RD, Nottingham, UK

[f]CITIMAC, University of Cantabria (UC), Avda. Los Castros s/n, 39005 Santander, Spain

*Corresponding author; e-mail: jonathan.albo@unican.es

Abstract

The slow kinetics in the photocatalytic reduction of CO_2, as well as the low quantum efficiencies achieved, directly related to the photocatalyst and reactor configuration applied, limit the widespread use of this technology. In light of this, the main objective of this work is to evaluate the continuous photocatalytic conversion of CO_2 into methanol in an optofluidic microreactor (with enhanced mass transport, large volume/active area ratio and uniform light distribution) using Cu nanoparticles synthesized in the hydrophilic 3-methyl-n-butylimidazolium tetrafluoroborate

(BMIm.BF_4) ionic liquid and embedded in TiO_2 (P25). The ionic liquid not only acts as a template to control the size of the nanoparticles but also as a stabilizing agent. The analysis includes the effect of structural parameters of the photoactive layer such as Cu content (from 0.8 to 6.8 wt.%) and photocatalyst loading (0.5-3 mg·cm^{-2}), as well as operating variables such as UV and visible light intensities (2.5-10 mW·cm^{-2}) and cell configuration (i.e. one or two compartments). The maximum methanol yield reached from the continuous transformation of CO_2 is r = 230.3 μmol·g^{-1}·h^{-1} at 2 wt.% Cu content, photocatalyst loading of 2 mg·cm^{-2}, UV light intensity of 10 mW·cm^{-2} and a two-compartment microreactor configuration. This result outperforms the values previously reported for Cu/TiO_2-based systems using optofluidic microreactors, as well as most of those in common CO_2 photoreactors.

Keywords: Optofluidic microreactor, Cu/TiO_2 photocatalyst, ionic liquids, CO_2 photoreduction, methanol.

1. Introduction

The CO_2 levels have raised from a pre-industrial level of about 270 ppm to surpass the 400 ppm threshold (413 ppm in August 2020) [1] and the new scenario puts energy-related CO_2 emissions on a slow upward trend to 2040, a trajectory far out of step with what scientific knowledge says will be required to tackle climate change. Extensive efforts have been paid to capture CO_2 from combustion streams including adsorption/absorption or membrane separation methods in a Carbon Capture and Storage (CCS) approach [2, 3]. However, in contrast to carbon sequestration that treats CO_2 as waste, Carbon Capture and Utilization (CCU) treats CO_2 as a resource [4, 5]. The reasons are simple, first profits since a robust market could be developed in the future to utilize

CO_2 as an industrial feedstock and hopefully absorbing decisive quantities of CO_2 away from the atmosphere.

There are different methods for the activation and transformation of CO_2, including chemical, thermochemical, biochemical, electrochemical or photochemical pathways [6]. The latter is an alternative with increasing attention that permits the conversion of CO_2 under mild conditions without additional energy input (except for the solar irradiation) [7]. Among the different products from the photocatalytic conversion of CO_2, methanol (CH_3OH) is of particular interest [8]. The photocatalytic reduction of CO_2 to CH_3OH can be considered a "killing two birds with one stone" approach since it gives the possibility to close the carbon loop and generate valuable chemicals from CO_2 in a circular economy. Besides, the process can be applied at mild conditions, in contrast to the conventional thermocatalytic process for CH_3OH production by reforming of CH_4 through syngas (H_2+CO).

Titanium dioxide (TiO_2), mainly in its anatase and rutile forms, has been the most widely used semiconductor for solar-fuel production, and particularly for the formation of CH_3OH [9-11]. This is because TiO_2 is a wide bandgap (~3 eV), cheap and nontoxic semiconductor made up of abundant elements and resistant to photocorrosion. Nevertheless, it is also well known that TiO_2 presents poor electron-hole pair separation. Among the different strategies to overcome this limitation, doping TiO_2 with a metal catalyst can be an effective and direct way to promote charge separation, CO_2 activation and selective formation of reaction products, inhibiting the back-recombination reaction [7]. In particular, doping TiO_2 with Cu has been proven to be a successful strategy for improving the photocatalytic efficiency of the CO_2 reduction process to CH_3OH [7, 10-12], that can be probably ascribed to the preference of H to adsorb on Cu and react with O of the co-adsorbed O-CH_3 intermediate, thereby forming CH_3OH [13]. Besides, Cu has the ability to

trap electrons, without affecting their mobility, and thus reduce recombination losses of the photogenerated charges and enhance photoconversion performance. For proper development of the CO_2 photocatalytic reduction technology, however, it is not uniquely required active and stable photocatalysts, but also efficient photoreactor designs to effectively harness the light irradiation required in the process and allow an optimised exposure of catalytically active sites to light. A number of different laboratory photoreactor designs have been assayed for the photocatalytic production of CH_3OH from CO_2, mainly including common slurry batch-type reactors [14]. These simple configurations have been demonstrated to be inefficient to induce the challenging reaction to form CH_3OH, due to a low surface-area-to-volume ratio because of particle agglomeration, and the required separation of the photocatalyst material from obtained products. Recently, the research in the so-called optofluidics, a synergy of microfluidics and optics (which has a distinct feature of fluids, light, and their interaction) may offer several advantages in the photocatalytic reduction of CO_2, including large surface-area-to-volume ratio, uniform light distribution, enhanced mass transfer and fine flow control [15]. Besides, the incorporation of optofluidics can greatly reduce the requirements for time, sample volume and equipment. Microreactors can be classified in several categories, such as micro-capillary, single microchannel, multi-microchannel and planar microreactors, where the latter are usually advantageous due to a larger photon receiving area. In fact, planar microreactor configurations have already exhibited superior performance in various photocatalytic processes, such as water splitting [16] or wastewater treatment [17]. To date, however, few works applied this microreactor configuration to carry out numerical simulations [18] or experimental analyses [12, 19-21] for the photocatalytic conversion of CO_2. Besides, only one of these previous reports takes advantage of the use of Cu/TiO_2-based materials (i.e. CuO-deposited TiO_2 nanorod thin films) [12], where the maximum CH_3OH

formation rate obtained is still modest (r = 36.2 μmol·g^{-1}·h^{-1}) under UV illumination and a reaction temperature of 80º C (which is an undesirable condition for practical applications). Therefore, a breakthrough to boost the photocatalytic hydrogenation of CO_2 into CH_3OH at ambient conditions is still to be seen.

In light of this, the main objective of the present study is to evaluate the performance of a planar optofluidic microreactor-based system including Cu nanoparticles (NPs) embedded in commercially available TiO_2 (P25) and supported onto carbon papers for the continuous photocatalytic conversion of CO_2 to CH_3OH under UV and visible light irradiation at ambient conditions. Among the different reported methods to prepare Cu NPs from their salts, the Cu NPs in this work are synthesized in hydrophilic 3-methyl-n-butylimidazolium tetrafluoroborate ($BMIm.BF_4$) ionic liquid (IL). ILs, and in particular imidazolium-based ILs, are one of the most versatile and environmentally sustainable media templates for the generation of a plethora of stable and naked colloidal mono-and bi-metallic NPs, conferring electrosteric stabilization through the formation of a semi-organized protective layer composed of ions surrounding the Cu NPs [22]. This allows first avoiding the use of capping agents that are usually difficult to remove from the surface of the NPs and decrease the catalytic activity, and also calibrating the shape, size and distribution of the metal NPs [23]. The work includes an evaluation of the stability and performance of the Cu/TiO_2 carbon papers, paying attention to the effect of structural parameters of the photoactive layer such as Cu content and photocatalyst loading, as well as operating variables such as light intensity (UV and Vis light) and cell configuration (i.e. one or two compartments) on the photochemical formation of CH_3OH. The research efforts in this work thus cover several of the key parameters in the process, and it can be seen as a step forward into the

development of more efficient systems for the continuous photocatalytic transformation of CO_2 to CH_3OH.

2. Material and methods

2.1. Synthesis and characterization of the Cu/TiO_2-based photocatalysts

The Cu NPs were prepared according to a previously reported method [23]. Typically, copper chloride dihydrate ($CuCl_2 \cdot 2H_2O$, 134 mg, 0.79 mmol) was dissolved in the hydrophilic IL (BMIm.BF_4) (3 mL) at room temperature during 30 min. Then, a solution of sodium borohydride ($NaBH_4$, 296 mg, 7.9 mmol) dissolved in methanol (3 mL) was added to the reaction mixture dropwise. The reaction mixture turned black due to the formation of the Cu NPs, which were washed with methanol (3 times, 5 mL) and dichloromethane (3 times, 5 mL). Afterward, the NPs were isolated by centrifugation (3500 rpm) and dried under vacuum. Subsequently, the isolated Cu NPs (3.3, 5.0, 6.2, 7.5 and 20 mg) were dispersed in dichloromethane (5 mL) and loaded in the desired amount (300, 200, 150, 150 and 100 mg, respectively) of TiO_2 (P25) to obtain the Cu/TiO_2 composites (wt/wt. %). After stirring at room temperature for 1 h, the obtained nanomaterials were isolated by centrifugation, washed with dichloromethane, dried under vacuum and stored under argon before use.

The structural characterization of the samples was performed by X-ray powder diffraction (PXRD) in air atmosphere on a Bruker D8 Advance diffractometer, using Cu Kα radiation and a LynxEye detector. Diffraction patterns were collected with an angular 2θ range between 20° and 100° with a 0.03° step size and measurement time of 3 s per step and a graphite monochromator. The instrumental resolution function (IRF) of the diffractometer was obtained from the LaB_6 standard. The spectrum analysis was done with EVA software (Bruker), comparing with the spectra of the

COD database. Transmission electron microscopy (TEM) measurements were performed using a JEOL 2100F FEG-TEM operated with an accelerating voltage of 200 kV. TEM samples were prepared using a nickel mesh holey carbon film TEM grids (Agar Scientific, UK). X-ray photoelectron spectroscopy (XPS) measurements were performed using a Kratos AXIS Ultra DLD instrument. High-resolution data on the C 1s, Ti 2p, O 1s, and Cu 2p photoelectron peaks were collected at pass energy of 20 eV over energy ranges suitable for each peak, and collection times of 5 min, step size of 0.1 eV. The high-resolution data were charge corrected to the reference C 1s signal at 284.8 eV. Micro Raman spectroscopy was performed using a Horiba Jobin Yvon LabRAM HR Raman spectrometer. Spectra were acquired using a 532 nm laser (at 20 mW power), a 100 x objective lens and a 200 μm confocal pinhole, using a Synapse CCD detector (1024 pixels) thermoelectrically cooled to −60 °C. The instrument was calibrated using the zero-order line and a standard Si(100) reference band at 520.7 cm^{-1}. UV-Vis diffuse reflectance measurements were performed with a CARY 5000 spectrophotometer. IR analyses were conducted using a Bruker Alpha FTIR (Fourier transform infrared) spectrometer with an ATR attachment. Data collection utilised 256 cumulative scans with a resolution of 4 cm^{-1}. Finally, N_2 isotherms of the catalysts, previously degassed at 180 °C under vacuum for 18 h, were obtained using TriStar and 3Flex Micromeritics instruments. Specific surface areas were determined by the BET multipoint method, and the average pore volume was obtained by the BJH method.

2.2. Preparation of the light-responsive papers

The light-responsive surfaces were manufactured by airbrushing a catalytic ink onto a teflonated porous carbon paper type TGP-H60 (Toray Inc.) covered by a paper mask with a hole of 1 cm^2, according to the scheme shown in Figure S1 (please see *Supplementary Information*). This ink includes the Cu NPs synthesized in ($BMIm.BF_4$) an embedded in TiO_2, the bare TiO_2 or the Cu

NPs, Nafion® dispersion 5 wt.% (Alfa Aesar) as binder and isopropanol (IPA) (Sigma Aldrich) as a vehicle, with a 70/30 catalyst/Nafion mass ratio and a 3 % solids (catalyst + Nafion) percentage; this mixture was sonicated for 30 min to obtain a homogeneous slurry that was subsequently airbrushed on the surface of the porous carbon paper. This chemically stable substrate present low thickness (0.19 mm) and high porosity (78%), which results in a high gas permeability (1900 ml·mm/(cm^2·h·mmAq)), contributing to an efficient transfer of CO_2 and diffusion of products [24]. The photoactive surfaces with different catalytic loadings (L = 0.5 - 3 mg·cm^{-2}), were prepared by simple accumulation of layers and complete IPA evaporation at 100 ºC on a heating plate. The catalyst loading was determined by the weight difference between the mass of the carbon paper before spraying and the mass of catalyst coated paper after different times. Before spraying the photoactive materials, poly-tetrafluoroethylene (PTFE) was sprayed on the other side of the carbon paper (1 mg·cm^{-2}) followed by calcination at 360 ºC for 1 h in air. This allows to increase the hydrophobicity of the material and prevents water leakage [19, 20]. Thus, the developed Cu/TiO_2 carbon papers perform the separation between the liquid and gas phases in the microchambers when using a two-compartment configuration. Table 1 shows the nomenclature used and the elemental composition of the photocatalysts determined by Microwave Plasma Atomic Emission Spectroscopy (MP-AES 4200 Agilent Technologies). All materials were dried at ambient conditions for 24 hours and rinsed with deionised water before use.

Table 1. Composition and metal loading of the prepared photoactive surfaces.

Photocatalyst	Nomenclature	Cu content (wt.%)	*L* (mg·cm^{-2})
TiO_2	TiO_2	-	2
Cu/TiO_2	Cu0.8	0.78	2
	Cu2	1.95	2
	Cu3.6	3.61	2
	Cu6.8	6.84	2
	Cu2(0.5)	1.95	0.5
	Cu2(1)	1.95	1
	Cu2(3)	1.95	3
Cu	Cu	100	2

2.3. Optofluidic microreactor and experimental conditions

The prepared Cu/TiO_2 carbon papers were employed as photoactive surfaces in the planar optofluidic microreactor (APRIA Systems S.L.). The reaction microchamber was 1 cm^2 and 75 µL, thus providing high surface-area-to-volume ratio, uniform light distribution, and mass transfer. The material was sandwiched with PTFE gaskets between two highly transparent (light transmission of 90% at >365 nm) polymethylmethacrylate, PMMA (Altuglas-Arkema) plates and a stainless-steel plate on the top. The light-responsive materials were placed in the centre of the reaction chamber of the PMMA plate (Figure S2 in *SI* for more details). A CO_2 saturated 0.5 M $KHCO_3$ (Panreac >97%) aqueous solution was prepared with ultra-pure water (18.2 MX cm at 273 K, MilliQ Millipore system) and supplied to the liquid microchamber with a peristaltic pump (Miniplus 3 Gilson) at a flow rate of Q_L = 50 µL·min^{-1}. In the two-compartment experiments, CO_2 (99.99 %) flows continuously in the gas microchamber controlled with a gas volumetric flowmeter

(Omega) at a flow rate of Q_g = 25 mL·min^{-1}. 1200 mW LEDs (LED Engin) with maximum intensities at wavelengths of 365 nm (UV) and 450 nm (Vis) lights, illuminated the liquid microchamber from the top through a window of 1 cm^2 to produce photo-excited electron-hole pairs for the reduction of CO_2 with water at the surface. As already mentioned, the experiments were carried out in two different microreactor configurations: (a) one compartment, with one inlet (solution + CO_2) and outlet (solution + CO_2 + products) and; (b) two compartments, with two different inputs (CO_2 as gas and solution) and one output (solution + CO_2 + products). Figure 1 schematically represents the lab scale plant for the continuous photoreduction of CO_2 to CH_3OH, while Figure 2 shows the microreactor for one and two-compartment configurations. The light intensity, E, varied from 2.5 to 10 mW·m^{-2}, measured by a radiometer (Photoradiometer Delta OHM) and controlled by adjusting the distance between the microreactor and the LED. The experiments were carried out in continuous mode under ambient temperature and pressure conditions. The microcell was placed in a ventilated dark box and the temperature was controlled with an infrared thermometer to ensure an ambient temperature (~25 ºC) during the experimental time.

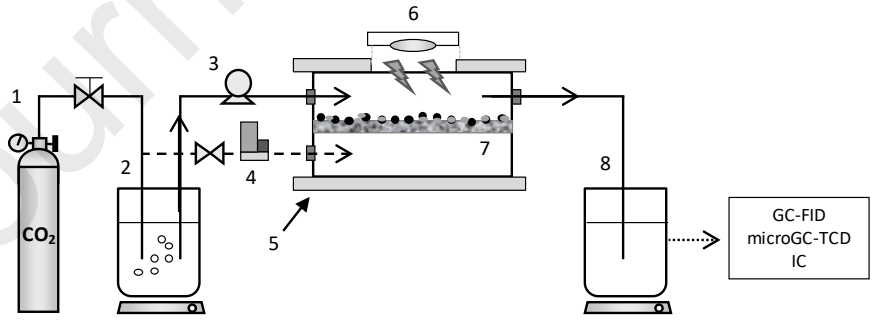

Figure 1. Scheme of the experimental setup.

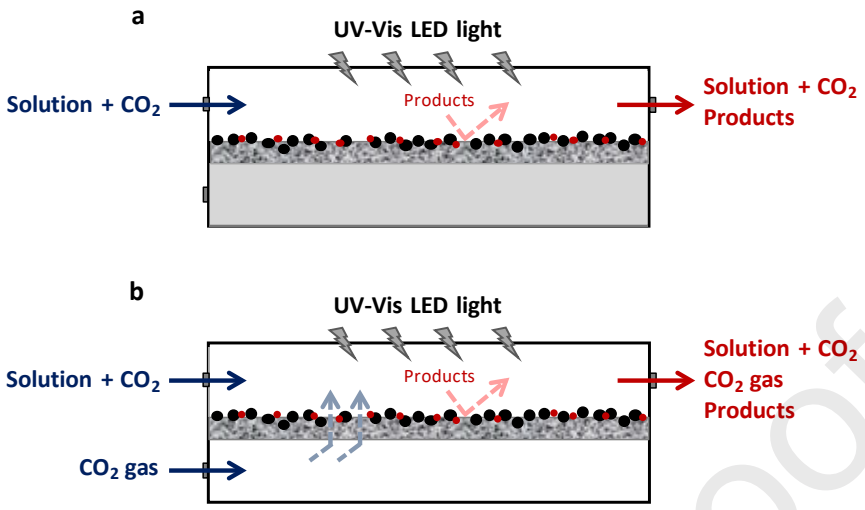

Figure 2. Microreactor in (a) one compartment and, (b) two-compartment configurations.

Sample aliquots were taken every 30 min and for 120 min from the collection vessel placed at the outlet of the microreactor. The concentration of alcohols in each aliquot was analysed in duplicate in a headspace gas chromatograph (GCMS-QP2010 Ultra Shimadzu) equipped with a flame ionization detector (FID). Formate ($HCOO^-$) concentration was analysed in duplicate by Ion Chromatography (Dionex ICS 1100). Gas-phase reduction products were analysed in line with a microGC 3000 (Inficon) equipped with a Thermal Conductivity Detector (TCD). An average concentration was obtained for each product from the performance of three replicates with an experimental error of less than 14.2 %. The performance for the photocatalytic conversion of CO_2 was evaluated in terms of formation rate, r, in $\mu mol \cdot g^{-1} \cdot h^{-1}$ (i.e., concentration obtained for every product at reactor outlet per photocatalyst amount and time), selectivity, S, defined as the ratio between reaction rates for different products and the cumulative reaction rate, and the Apparent Quantum Yield, AQY:

$$AQY\ (\%) = \frac{n_e}{n_p}\ x\ 100 \qquad (1)$$

where n_e is the rate of electrons transferred towards a certain product, calculated by multiplying the number of molecules evolved (mol) by the number of reacted electrons (i.e. 6 e^- for CH_3OH and 12 e^- for C_2H_5OH) and the Avogadro´s number (mol^{-1}); and n_p is the rate of incident photons on the surface, calculated by multiplying the power density of the incident light ($W \cdot m^{-2}$) by the irradiation area (m^2), reaction time (s) and wavelength peak (m), divided by the Planck's constant ($J \cdot s^{-1}$) multiplied by the speed of light ($m \cdot s^{-1}$).

3. Results and discussion

3.1. Characterization of the Cu/TiO_2-based photocatalysts

The Cu NPs were prepared by reduction of copper chloride dehydrate in hydrophilic ($BMIm.BF_4$) IL using $NaBH_4$. These NPs were isolated and embedded into commercially available TiO_2 (P25) by impregnation and characterized by powder X-rays diffraction (PXRD), transmission electron microscopy (TEM), X-ray photoelectron spectroscopy (XPS) and UV-visible absorption. First, the semiquantitative PRXD analyses of the Cu-based and Cu/TiO_2 photocatalysts was performed using the pattern matching routine of Diffrac Plus-EVA (Bruker). The Cu-based NPs display Cu_2O and CuO as mayor crystalline phases with the presence of a small quantity of Cu metal. Besides, the composites show anatase and rutile TiO_2 polymorphs in the ratio 4:1, which is consistent with Raman spectra (Figure S3 in *SI*). This is in anatase content range previously observed for an optimal photocatalytic activity [25], although the intense debate on the right polymorph composition and the origin of this synergism still continues. Cu doping does not alter the crystalline structure of TiO_2 (please see Figure S4 and Table S1 in *SI).* TEM images show Cu NPs deposited onto TiO_2 with a size ranging between 3-5 nm for the highest Cu concentration (6.8%

Cu/TiO_2), whereas for lower Cu content (0.8 and 2% Cu/TiO_2) Cu NPs were not clearly observed by TEM (Figure 3) although detected via EDX analyses (Figure S6 and S7 in *SI*). These results suggest the formation of small Cu clusters (e.g. < 1 nm) for low Cu concentration in TiO_2 since Cu NPs were not clearly observed using cold-field emission gun TEM (non-spherical-aberration-corrected) possibly due to the low contrast difference between Cu and Ti atoms, which prohibits the atomic scale investigations via traditional TEM, hiding the presence of Cu clusters.

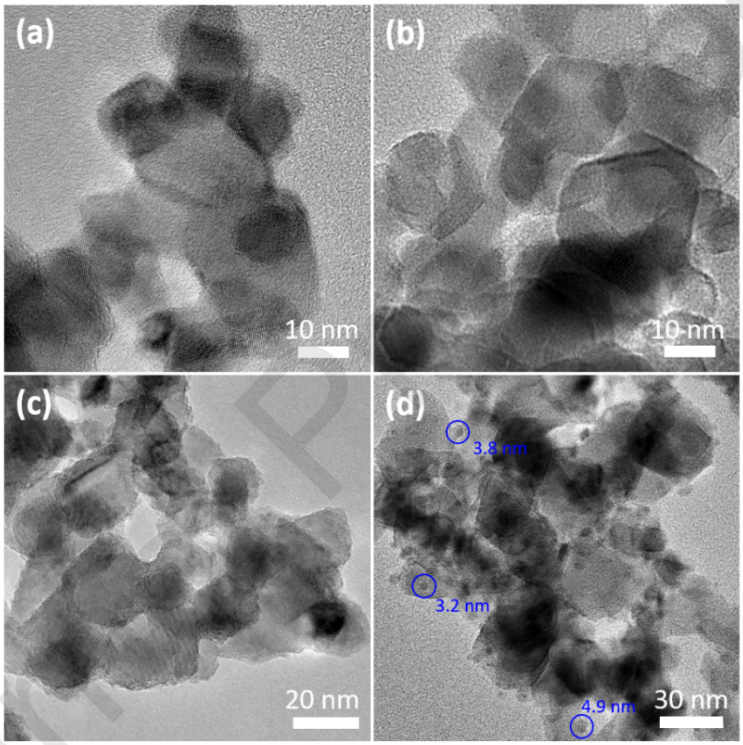

Figure 3. TEM images of (a) TiO_2, (b) 0.8% Cu/TiO_2, (c) 2% Cu/TiO_2, and (d) 6.8% Cu/TiO_2.

XPS measurements of Ti 2p core (Figure 4a) showed peaks at 458.5 eV and 464.4 eV for all samples, which can be ascribed to Ti^{4+} ions in TiO_2 [26]. XPS measurements of Cu $2p_{3/2}$ region displayed a broad peak at ca. 932 that can be assigned to a mixture of valence states of Cu_2O and CuO (Figures 4 and S8, Table S2 in *SI*) [27]. The ratio between Cu_2O and CuO was estimated,

showing an increase of CuO with the increase of Cu content in the composite, which is evidenced by the strong satellite peak observed for 6.8% Cu/TiO_2 photocatalyst that is associated with CuO, in agreement with PXRD results (Table S1 in *SI*). These results indicate that Cu(II) valence state is preferentially stabilised for higher Cu contents in the TiO_2 matrix, which might be due to the presence of IL in the synthesis of the Cu NPs [28].

UV–Vis diffuse reflectance spectroscopy (Figure 5a) showed that the absorption band edge for TiO_2 is around 400 nm and the addition of Cu NPs makes the absorption increasing at longer wavelengths (visible range), as observed from the absorption edge of 440 nm with Cu6.8. It can be also seen that increases in Cu content led to an enhanced absorbance in the Cu/TiO_2 samples. This characteristic can be attributed to the presence of Cu oxide species (as seen in PXRD and XPS) and their d-d transitions [29]. Figure 5b shows the estimated optical bandgap energies of the samples as calculated by Kubelka- Munk method ([F(reflectance, R)$h\nu$]^2 vs. photon energy ($h\nu$)). Firstly, low bandgap energy values ranging from 2.86 and 2.96 eV can be obtained for the Cu/TiO_2 composites compared to 3.11 eV for TiO_2 that can be assigned to the presence of Cu_2O and CuO, which are *p*-type semiconductors with small bandgap energies (i.e. 1.93 eV for the Cu NPs). The narrowing in bandgap energy with Cu content can be linked to an improved electronic properties of the composites as a results of the interaction between the dopant metal and TiO_2.

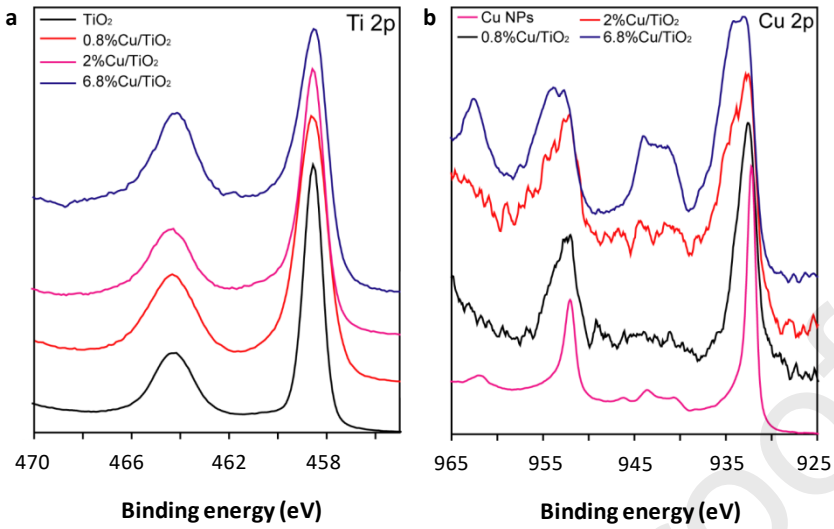

Figure 4. XPS spectra of TiO_2, Cu/TiO_2 and Cu samples: (a) Ti 2p and (b) Cu 2p.

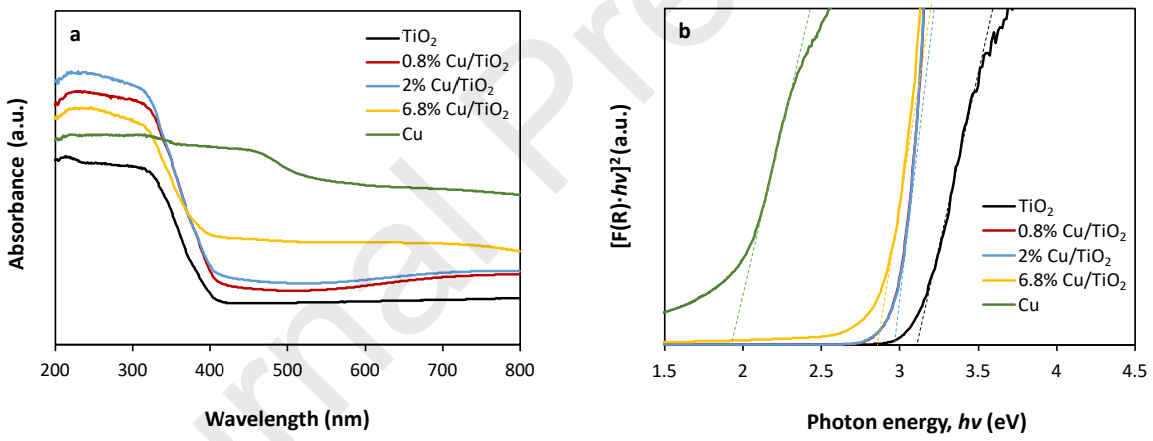

Figure 5. (a) UV-Vis absorption spectra and, (b) bandgap energies plot (Kubelka-Munk function) of TiO_2, Cu/TiO_2 and Cu samples.

Besides, FTIR analyses show three characteristic peaks at 3370, 1630 and 650 cm^{-1} associated with stretching vibrations of hydrogen-bonded water molecules and hydroxyl groups, bending vibrations of O-H group and Ti-O-Ti bridging stretching mode, respectively [30]. It is of note that

there is no C-H and C-N stretching observed in FTIR, which evidenced the absence of ionic liquid on the surface of the Cu/TiO_2 photocatalysts (Figure S9 in *SI*). Finally, BET analysis (Figure S10 and Table S3 in *SI*) showed that BET surface area and pore volume of the materials slightly decreased from 58.6 $m^2 \cdot g^{-1}$ and 0.110 $cm^3 \cdot g^{-1}$ to 56 $m^2 \cdot g^{-1}$ and 0.104 $cm^3 \cdot g^{-1}$ for Cu0.8 and Cu2, respectively. The values reached a minimum of 46.8 $m^2 \cdot g^{-1}$ and 0.0.097 $cm^3 \cdot g^{-1}$ as the loading of Cu NPs in TiO_2 was increased (Cu6.8).

3.2. Continuous transformation of CO_2 in the planar optofluidic microreactor

The micro-optofluidic system including the Cu NPs embedded in TiO_2 led predominantly to the formation of CH_3OH, with ethanol (C_2H_5OH) as the second alcohol, and also HCOOH, which is a probable intermediate in the CO_2 conversion pathway to CH_3OH [5, 13]. Additionally, small quantities of CO and CH_4 were detected (AQY<0.05%), which is not unexpected for Cu-containing TiO_2 surfaces [31]. Blank tests were also conducted in the dark and the absence of CO_2 and no CO_2-reduction products were detected. Figure 6 shows the yields for CH_3OH with irradiation time and the number of consecutive runs for Cu2 photocatalyst (L = 2 $mg \cdot cm^{-2}$). The reaction solution was changed after each run. Moreover, Table 2 shows the Cu/TiO_2 weight in Cu2 after 2, 4 and 8 hours of CO_2 photoreduction time. The total initial weight of Cu/TiO_2 placed in the Cu2-based carbon paper was 2 mg.

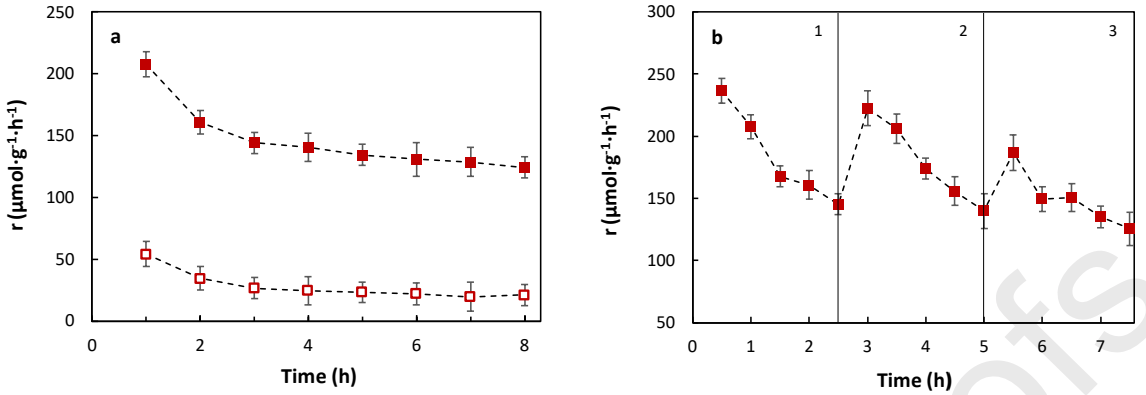

Figure 6. Time course for the (a) photocatalytic production of CH_3OH using Cu2 under UV (■) and Vis (□) light and, (b) after three consecutive runs under UV.

Table 2. Weight loss for Cu2-based carbon papers after a CO_2 photoreduction period of 2, 4 and 8 hours.

Time (h)	Cu2 (mg)		Weight loss (%)
	Initial	Final	
2	2	1.91	4.5
4		1.8	10
8		1.69	15.5

As observed in Figure 6a, the activity of Cu2 decays more abruptly during the first 2 hours of irradiation, going from r = 207.8 μmol·g^{-1}·h^{-1} to r =165.9 μmol·g^{-1}·h^{-1} and from r = 54.1 μmol·g^{-1}·h^{-1} to r = 34.4 μmol·g^{-1}·h^{-1} under UV and Vis light irradiation, respectively. Beyond this point, the yields decay slowly after 8 hours of continuous photoreduction of CO_2, which may be related with the use of ($BMIm.BF_4$) in the synthesis that acts as stabilizing agent. The phenomenon of reduction in CH_3OH photoproduction with longer periods of light irradiation is commonly attributed to the reduction in photocatalyst ability to absorb light due to particle detachment, the

formation of intermediate un-desorbed products that block the active sites, or CH_3OH reforming (i.e. CH_3OH can act as hole scavenger itself, removing OH^- and resulting in a reduction of electron-hole recombination or the back reaction of O_2 and H_2) [32-34]. Besides, an initial reduction in catalytic efficiency for CO_2 photoreduction is commonly observed when applying Cu-modified TiO_2 materials (which is attributed to the change of the Cu oxidation state under catalytic conditions) after which pseudo-stable production rates can be achieved [35].

In any case, the results from Table 2 may indicate that the deactivation observed with the photoactive Cu2-based surfaces after 2 h of photocatalytic reaction can be mostly linked to material leaching from the carbon paper during operation, as we reported before for spray-coated Cu NPs onto porous carbon supports [24]. It is also important to notice that the photocatalyst surface changes from dark grey to greenish-white, which could be initially associated to the formation of Cu_2O during the experimental time, although it has probably more to do with the transformation of CuO to malachite ($CuCO_3.Cu(OH)_2$) as previously reported [36] since CuO is not stable in the reduction of CO_2 in water. Besides, Figure 6b shows how the yields decay progressively after three consecutive runs of 2.5 hours. Despite that, the increase at the initial stage of each cycle suggests that the activity loss can be also partially associated with the blocking of the photocatalytic sites, which is mitigated from one cycle to the other upon washing of the material. Thus, CH_3OH yield at the initial stage of the second cycle is 94 % of the initial yield in the first one and results in the 79 % in the third run. Based on this, the results presented hereafter are for one run and 2 h of irradiation, where pseudo-steady conditions can be reached.

3.3. Effect of Cu content on process performance

The effect of Cu loading in the formation rates for CH_3OH, together with C_2H_5OH and HCOOH, is shown in Figure 7, while Figure 8 shows reaction selectivity to alcohols (CH_3OH and C_2H_5OH)

with TiO_2, Cu and the different Cu/TiO_2 photocatalytic composites tested under UV and Vis light illumination.

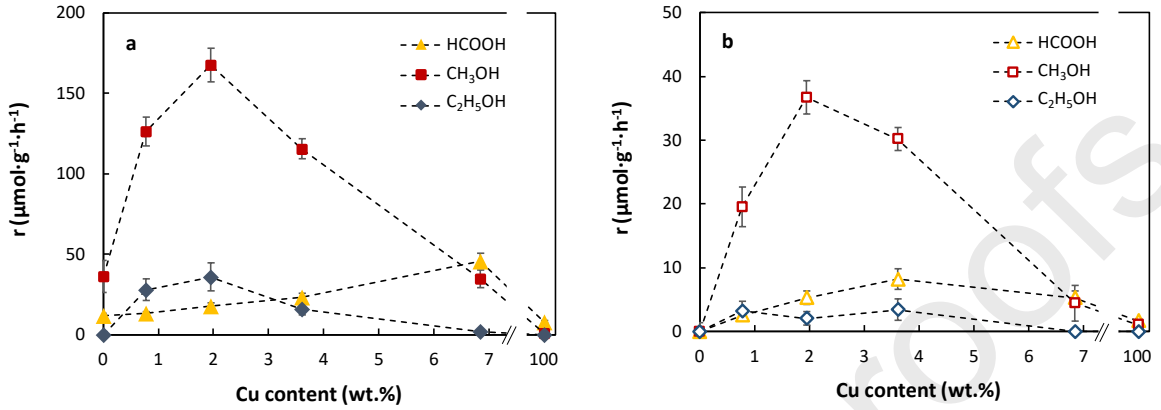

Figure 7. Yields for CH_3OH, C_2H_5OH and HCOOH in the photocatalytic reduction of CO_2 at different Cu contents and under (a) UV and (b) Vis light illumination.

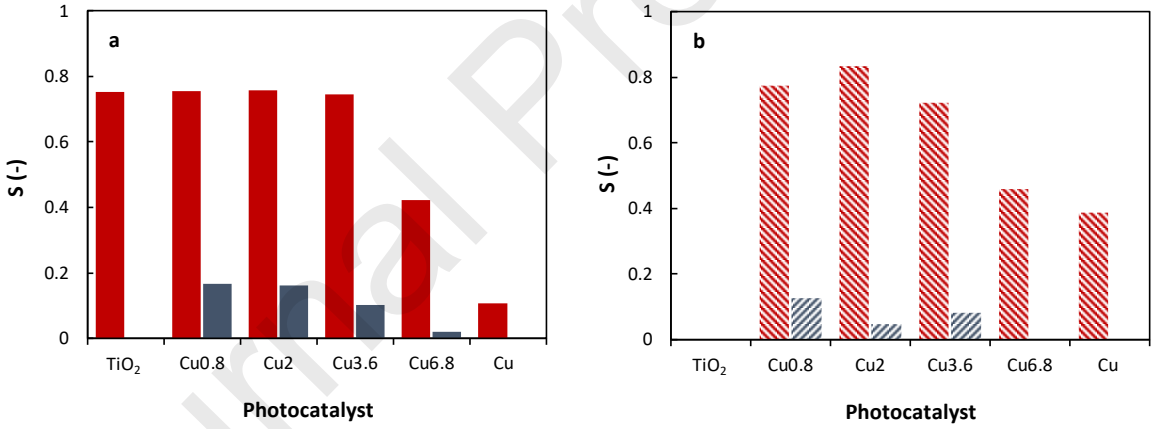

Figure 8. Selectivity of the reaction at increasing Cu content for CH_3OH (in red) and C_2H_5OH (in blue) under (a) UV and (b) Vis light illumination.

The results firstly show that yields for CH_3OH (and also for C_2H_5OH) can be increased with Cu loading until 2 wt.% (Cu2), in similarity with the optimum Cu content reported for other Cu/TiO_2-based systems in the production of CH_3OH [37-45]. At this optimal point, the CH_3OH yield is r =

167.5 μmol·g^{-1}·h^{-1} (*AQY* = 3.7 %) after 2 hours of UV illumination (Figure 7a). The same can be said under Vis light illumination (Figure 7b) where *r* for CH_3OH can be as high as *r* = 36.7 μmol·g^{-1}·h^{-1} (*AQY* = 0.7 %). It is also worth revealing that the formation of CH_3OH is 4.6 fold higher than that production rate achieved over bare TiO_2 (P25) under UV illumination (*r* = 36.1 μmol·g^{-1}·h^{-1}, *AQY* = 0.8 %). As expected, no CH_3OH was detected with TiO_2 under Vis illumination. Thus, doping with the Cu NPs may be responsible for the Vis light activity, where probably the electrons generated on the Cu conduction band can be easily injected into the inactivated TiO_2, enhancing charge separation [12, 31, 46, 47]. In spite of this, the absorption of incident light with the Cu-doped TiO_2 samples remains significantly higher under UV light than under visible light illumination as expected for TiO_2 (P25). This means that upon light absorption, the materials applied are able to generate more electron-hole pairs under UV light, resulting in an enhanced CO_2 photoreduction performance.

Moreover, the fact that the rates and *AQYs* for CH_3OH obtained at Cu (*r* = 0.94 μmol·g^{-1}·h^{-1} and *AQY* = 0.02% under UV illumination; *r* = 1.03 μmol·g^{-1}·h^{-1} and *AQY* = 0.018% for Vis light illumination) are also remarkably lower than those values reached with the Cu/TiO_2 composites, demonstrates the favoured interplay between the Cu NPs synthesized in IL and TiO_2, that probably act together as active sites for CO_2 photoreduction. PXRD and XPS analyses demonstrated the presence of Cu_2O. Cu_2O is a *p*-type semiconductor with a narrow bandgap (ca. 2 eV) [48] that has been proved to be an active catalyst for CO_2 conversion to alcohols [5, 7, 10-12] and in particular in the photocatalytic conversion of CO_2 to CH_3OH under Vis light [46, 49]. In general, the enhancements in yields and efficiencies with Cu content, which is a well-known material for the production of alcohols [5, 7, 9-12], can be firstly explained by a higher amount of Cu sites available for CO_2 transformation. The results from previous reports demonstrated that the tight contact of

TiO_2 with Cu may cause a redistribution of electric charges. Cu can serve as an electron trapper, without affecting its mobility, and prohibits the recombination of electron and hole, significantly increasing photoefficiency, as also confirmed with UV-Vis absorption (Figure 5). Moreover, the rapid transfer of excited electrons in the presence of Cu enhances the separation of electrons and holes [31, 35, 39, 41]. Unfortunately, higher Cu contents cannot further increase the production of CH_3OH. This can be firstly explained by a shielding effect of the TiO_2 surface reducing the photoexciting capacity and thereby weakening photocatalytic activity of the composites, together with a reduction in BET surface area as Cu content increases in the composite materials. This effect can be also associated with a decrease in the Cu_2O/CuO ratio with increases in Cu content (as observed from PXRD and XPS), since CuO is usually more selective to CH_4 and CO formation [50]. This change in Cu_2O/CuO can be linked to the use of ($BMIm.BF_4$) IL in the synthesis of the Cu NPs [28].

In accordance with Figure 7, the results presented in Figure 8 evidence that Cu content has a marked effect on reaction selectivity at the Cu/TiO_2 photoactive surfaces developed. In particular, the data show that a Cu content between 0.8 % to 3.6 % (Cu0.8-3.6) seems to be beneficial for the conversion of CO_2 to CH_3OH and C_2H_5OH over HCOOH production, with an *S* of 0.77 and 0.15, respectively. When exceeding a 3.6 wt.% Cu content (Cu3.6-Cu), the photocatalyst tends to enhance the production of HCOOH, which has been also reported before at Cu-containing TiO_2 surfaces [7, 9, 10]. This led to a decrease in CH_3OH production, indicating that the amount of Cu active sites in the photoactive surface have a critical influence on reaction selectivity (and so in reaction mechanisms). Overall, the optimum amount of Cu in the photocatalyst has been proved to be 2 wt.% (Cu2) for an efficient and selective formation of CH_3OH (r = 167.5 $\mu mol \cdot g^{-1} \cdot h^{-1}$, AQY = 3.7%, S = 0.77) under the experimental conditions tested.

3.4. Effect of photocatalyst loading and light intensity

Photocatalyst loading can affect not only the transport of CO_2, OH^- and photons inside the active layer but it may also modify the active area available for the photoconversion of CO_2 to CH_3OH [19]. Thus, Figure 9 analyses the effect of a Cu2 loading ranging from $L = 0.5$ mg·cm^{-2} to 3 mg·cm^{-2} (Cu2(0.5) - Cu2(3)) on the reaction rates and concentrations obtained for CH_3OH and C_2H_5OH.

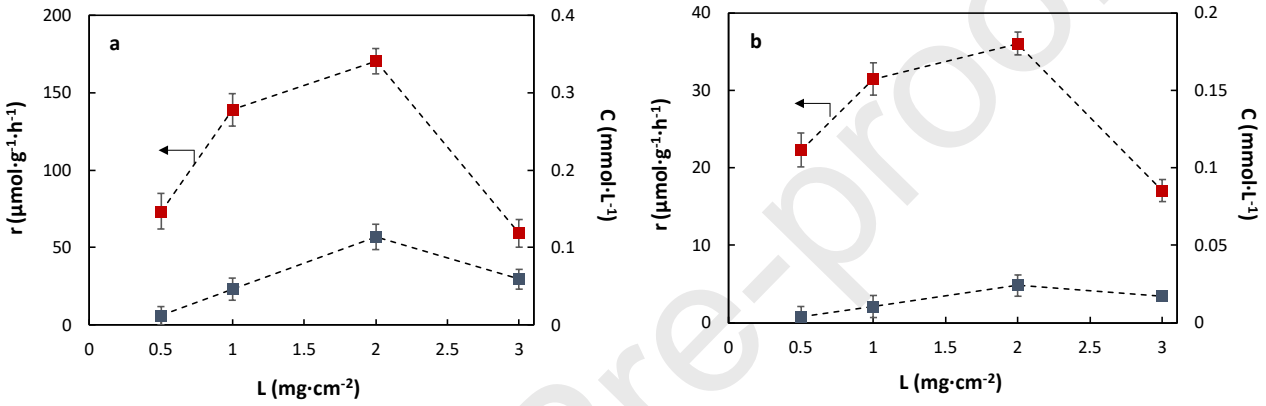

Figure 9. Effect of photocatalyst loading on CH_3OH (in red) and C_2H_5OH (in blue) production under (a) UV and (b) Vis light illumination.

From Figure 9, the production of CH_3OH per gram of Cu2 can be clearly enhanced when the loading increased from $L = 0.5$ to 2 mg·cm^{-2}, going from $r = 73.4$ µmol·g^{-1}·h^{-1} to $r = 167.5$ µmol·g^{-1}·h^{-1}, and from $r = 22.3$ µmol·g^{-1}·h^{-1}to $r = 36.1$ µmol·g^{-1}·h^{-1}for UV and Vis light illumination, respectively. The same can be observed for the yields to C_2H_5OH. At lower catalyst loading (below $L = 2$ mg·cm^{-2}), a reduced number of electron-hole pairs are probably generated due to the low photoactive surface available resulting in lower yields. As photocatalyst loading increases from 2 to 3 mg·cm^{-2}, the performance of the planar optofluidic microreactor-based system worsens, which can be probably associated not only to particle agglomeration, which led to a reduction in the photoactive surface available and a shadow effect but also to an increase in photocatalyst layer

thickness which can cause mass transfer resistance (also due to a probable formation of boundary layers), leading to more difficult access of reactants and photons [45]. Those effects together produce a reduction in CH_3OH yield of 65 % at Cu2(3) in comparison to the value achieved at the optimal photocatalyst loading of L= 2 mg·cm^{-2} (Cu2) under UV illumination.

In addition, the adjustment of the incident light intensity is key for optimal continuous production of CH_3OH in the photocatalytic microreactor. Figure 10 shows the yields and *AQYs* for CH_3OH in a light intensity range from E = 2.5 mW·cm^{-2} to E = 10 mW·cm^{-2} under UV and Vis light illumination. It should be noted that the microreactor remains close to ambient temperature during the experimental time.

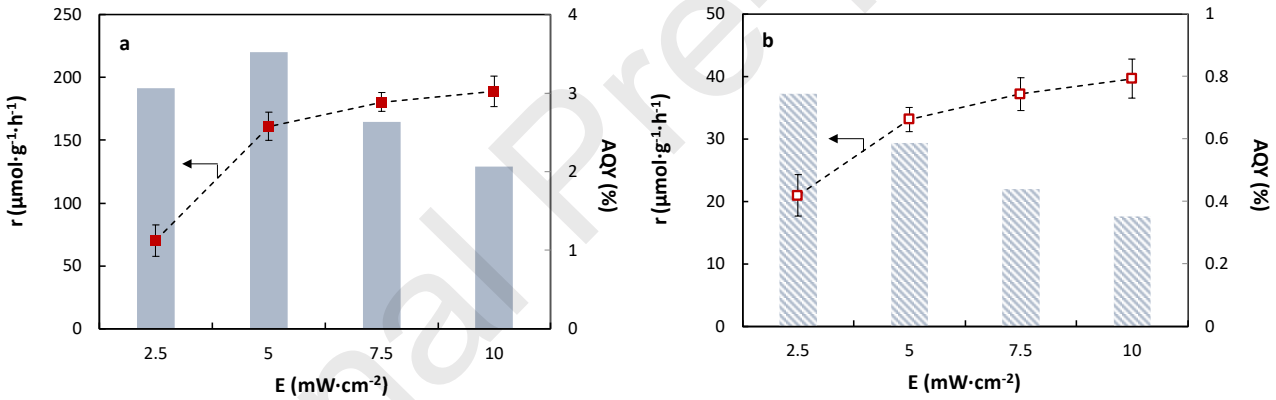

Figure 10. Rates and *AQYs* for CH_3OH production at different light intensities of (a) UV and (b) Vis LED lights.

It can be concluded that CH_3OH production can be still enhanced when increasing E from 5 to 10 mW·cm^{-2}, achieving a maximum r = 189.1 μmol·g^{-1}·h^{-1} under UV light. This can be easily explained as the increased light can generate more electron-hole pairs for the photocatalytic reduction of CO_2 to CH_3OH. In any case, beyond E = 5 mW·cm^{-2}, increases in light intensity are not proportionally reflected on CH_3OH concentration. This can be clearly seen in *AQY* evolution

from 5 to 10 mW·cm^{-2}, that decreases from AQY = 3.7 % to AQY = 2.1 % and from AQY = 0.6 % to AQY = 0.4 % for UV and Vis light, respectively, which might be explained by the consumption of additional incident photons for side reactions and a higher electron-hole recombination rate. Worth also mentioning that further increases in light intensity would not necessarily bring higher CH_3OH yields, since other factors (i.e. actives sites, irradiation time, reaction solution, reactor configuration, operational flows, etc.) may be key in defining the maximum production attainable in the system [7, 11]. The maximum yield achieved with Cu2 is therefore r = 189.1 μmol·g^{-1}·h^{-1} (AQY = 3.7 %) under UV with an intensity of E = 10 mW·cm^{-2}.

3.5. Effect of microreactor configuration

Table 3 compares the yields for CO_2 reduction in one and two-compartment (CO_2 supplied as gas) configurations under UV light (E = 10 mW·cm^{-2}) at Cu2 surfaces. The table includes the results obtained in a CO_2-saturated 0.5 M $KHCO_3$ solution when N_2 gas is supplied in the gas compartment (instead of CO_2) at a flow rate of 25 mL·min^{-1}.

Table 3. Photocatalytic reduction of CO_2 in one and two-compartment configurations under UV light.

Config.	**Flowing gas**	***r* (μmol·g^{-1}·h^{-1})**			***S* (-)**	
		HCOOH	*CH_3OH*	*C_2H_5OH*	*CH_3OH*	*C_2H_5OH*
Two compartments	CO_2	23.5	230.3	87.1	0.68	0.26
	N_2	21.8	216.8	56.5	0.73	0.19
One compartment	-	21	189.1	41.9	0.75	0.17

The production rates for liquid products in a two-compartment configuration demonstrated that the supply of additional CO_2 contributed to a higher photolysis efficiency with the Cu/TiO_2

composites. Specifically, the production of CH_3OH can be as high as r = 230.3 μmol·g^{-1}·h^{-1} (AQY = 2.5 %) in a two-compartment configuration, which implies that process performance can be still significantly enhanced by increasing CO_2 availability in the light-responsive Cu2 surface, in contrast to that value obtained with bare TiO_2 (P25) under the same conditions (r = 41.4 μmol·g^{-1}·h^{-1}, AQY = 0.4 %) that results only slightly improved. The fact that the values are also enhanced when N_2 is supplied in the gas compartment suggests that the data cannot be uniquely explained by an increase in CO_2 (adsorbate) availability on the photocatalytic surface, but also to an enhanced agitation of reactants in the microreactor, leading to increases concentration of CH_3OH. The two-compartment configuration may also provoke that products diffuse more easily, enhancing their concentration at the reactor outlet.

The results also suggest that the microreactor configuration may be able to vary reaction selectivity, where S to CH_3OH slightly declines to S = 0.68 when additional CO_2 is supplied as gas, while S to C_2H_5OH increases from S = 0.17 to S = 0.26. This may be explained by the effect of CO_2 in the vicinity conditions of the photoactive material, which might alter the catalytic mechanisms and provoke the formation of more reduced species [24]. Certainly, an in-depth study on reaction mechanisms is required to elucidate and control reaction selectivity in the photoconversion of CO_2 to CH_3OH, although important efforts have been already done [13, 18].

3.5. Comparison with other Cu/TiO_2-based systems

Finally, Figure 11a compares the highest yield obtained at Cu2 in the planar optofluidic microreactor, with other Cu/TiO_2-based systems for CH_3OH production reported over the years [12, 31, 32, 37-47, 51-70]. In addition, Figure 11b compares the yields normalized by the production of CH_3OH obtained over bare TIO_2 (P25) (when data available) so that the properties

of the Cu/TiO_2 photocatalyst applied can be discriminated from other variables such as reactor configuration, reaction solution or operating conditions [38-43, 45, 53].

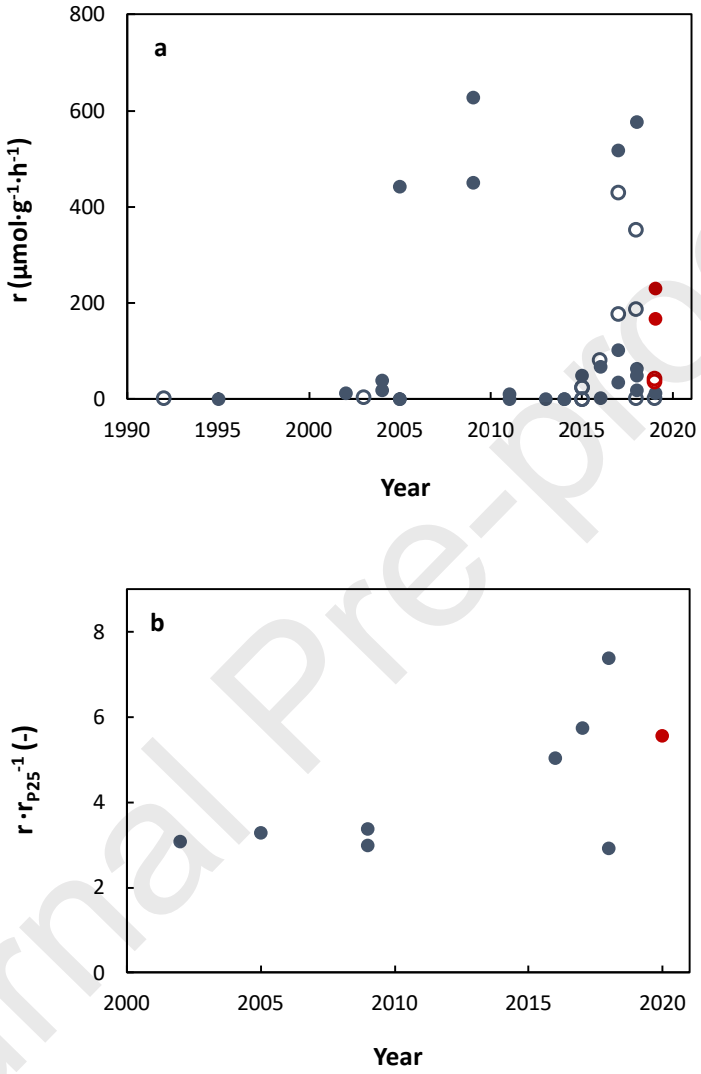

Figure 11. Evolution of normalized (a) *r*, and (b) $r \cdot r_{P25}^{-1}$ for CH_3OH over the years for different Cu/TiO_2-based systems in the photocatalytic reduction of CO_2 under UV (●) and Vis (○) light illumination. The values obtained in this work are in red.

As can be seen, the values obtained in the tested planar microreactor-based system with Cu2 photocatalyst outperformed most of those values observed at Cu containing TiO_2-based systems in literature for CH_3OH production (please see Table S4 in *SI*), which may denote the positive effect of applying a planar optofluidic microreactor configuration with enhanced mass transport, larger volume/active area ratio and uniform light distribution. In particular, the maximum formation rate obtained in this study (r = 230.3 $\mu mol \cdot g^{-1} \cdot h^{-1}$) is clearly higher than that found (r = 36.2 $\mu mol \cdot g^{-1} \cdot h^{-1}$) in the current state-of-the-art Cu/TiO_2-based optofluidic microreactor systems, when using a similar optofluidic microreactor and CuO (1.5 wt.%)-TiO_2 nanorod thin films as photocatalyst illuminated with UV light and a reaction temperature of 80º C [12]. This reveals the potential of the Cu NPs synthesized in ILs and embedded in TiO_2, as well as the optimized reactor configuration and operational variables, applied in this work for the continuous formation of CH_3OH at ambient conditions. Nevertheless, the values lag behind those achieved with other Cu/TiO_2-based materials suspended in the reaction media in slurry batch reactors under UV (values ranging from r = 442.5 to r = 627 $\mu mol \cdot g^{-1} \cdot h^{-1}$) and Vis light irradiation (from r = 352.9 to 429 $\mu mol \cdot g^{-1} \cdot h^{-1}$) [38, 39, 56], which can be ascribed first to the effect of doping the Cu/TiO_2 composites with other non-metallic materials (i.e. carbon, silica or g-C_3N_4) that are able to enhance the photoresponse by narrowing the bandgap energy of TiO_2 and improve the access of reactants to the actives sites [33, 34]; and then, to the effect of using specific reaction medium (i.e. acetonitrile/triethanolamine), able to promote the formation of CH_2 that eventually links up with OH^- to form CH_3OH [42]. Moreover, Figure 11b further confirms the ability of Cu2 (Cu NPs synthesized in ILs and embedded in TiO_2 (P25)) to conduct the continuous photocatalytic transformation of CO_2 into CH_3OH under UV light illumination, which is only surpassed by the normalized rate ($r \cdot r_{P25}^{-1}$) achieved by Y. N. Kavil and collaborators [38, 39] over Cu/C-co-doped

TiO_2 nanoparticles, which may be explained by the bandgap narrowing produced with carbon doping. In any case, it is also important to mention that these previous systems do not operate in continuous mode, and the obtained products need to be separated from the photocatalytic material at the reactor outlet, which makes them less suitable for a practical application of the photocatalytic reduction of CO_2.

All in all, the high CO_2 photoconversion rates and selectivities to CH_3OH obtained in this continuous flow microreactor-based system with Cu NPs synthesized in ($BMIm.BF_4$) and embedded in TiO_2 look promising, and can be seen as a step further in the development of efficient CO_2 photoreduction processes and devices.

4. Conclusions

In this work, a system based on a planar optofluidic microreactor and Cu nanoparticles synthesized in hydrophilic 3-methyl-n-butylimidazolium tetrafluoroborate ($BMIm.BF_4$) ionic liquid and embedded in TiO_2 has been applied for a more efficient photocatalytic conversion of CO_2 to CH_3OH, with C_2H_5OH and HCOOH as main secondary products.

The results firstly demonstrated that the activity of the prepared Cu/TiO_2-based carbon papers remains pseudo-stable after 8 hours of operation. Then, the yields for CH_3OH increased with Cu content up to 2 wt.% (r = 167.5 $\mu mol \cdot g^{-1} \cdot h^{-1}$, AQY = 3.7 %), clearly enhancing the values obtained at bare TiO_2 (r = 36.5 $\mu mol \cdot g^{-1} \cdot h^{-1}$, AQY = 0.8 %) under UV. This is explained by a higher availability of Cu sites for CO_2 conversion, as well as an enhanced redistribution of electric charges caused by Cu. The formation rates and $AQYs$ for CH_3OH obtained at Cu are additionally significantly lower than those reached with Cu/TiO_2 composites, which demonstrate the favoured interplay of TiO_2 and the Cu nanoparticles synthesized in IL. Doping TiO_2 with Cu nanoparticles

also made the photocatalyst to present activity in the visible region. Besides, CH_3OH production found an optimum at a catalyst loading of 2 $mg \cdot cm^{-2}$. Higher loadings probably led to particle agglomeration, reducing the photoactive surface and limiting the access of CO_2 and OH^-. The formation rates could still be enhanced by increasing light intensity up to 10 $mW \cdot cm^{-2}$, although the *AQY* fell as the additional incident photons may be consumed by side reaction and a higher electron-hole recombination occurs. Interestingly, a two-compartment microreactor configuration allowed achieving a higher CH_3OH production ($r = 230.3$ $\mu mol \cdot g^{-1} \cdot h^{-1}$, $AQY = 2.5$ %), also varying product selectivity under identical conditions. Thus, when CO_2 was supplied as gas in a two-compartment configuration, CH_3OH declines in favour of C_2H_5OH formation, which can be probably explained by the alteration provoked by CO_2 in the vicinity conditions of the photoactive material.

The high photoconversion rates and selectivities of CO_2 to CH_3OH conversion obtained in this continuous flow planar microreactor with Cu/TiO_2-based carbon papers at ambient conditions outperformed most of the values previously reported with Cu/TiO_2 in common photoreactor configurations and also in previous optofluidic microreactor systems, showing the benefits of both, the microreactor configuration and the Cu nanoparticles synthesized in (BMIm.BF_4) and embedded in TiO_2 applied in this work.

Acknowledgments

The authors gratefully acknowledge the financial support from the Spanish Ministry of Economy and Competitiveness (MINECO) under Ramón y Cajal programme (RYC-2015-17080), as well as PID2019-104050RA-I00 and MAT2017-83631-C3-3-R projects. M. I. Qadir and J. Dupont thank the CAPES (158804/2017-01 and 001), FAPERGS (16/2552-0000 and 18/2551-0000561-4) and

CNPq (406260/2018-4, 406750/2016-5 and 465454/2014-3) for their financial support. M. I. Qadir also acknowledges support from the European Union's Horizon 2020 research and innovation program under grant agreement No 810310, which corresponds to the J. Heyrovsky Chair project ("ERA Chair at J. Heyrovský Institute of Physical Chemistry AS CR – The institutional approach towards ERA") during the finalization of the paper. J. Alves Fernandes and M. Samperi thank the Nanoscale and Microscale Research Centre (nmRC) in Nottingham; and Beacons of Excellence: Propulsion Futures and Green Chemicals. J. Alves Fernandes is also grateful to Dr. Graham A. Rance from nmRC for assistance with Raman spectroscopy analysis.

References

[1] Mauna Loa Observatory – National Oceanic and Atmospheric Administration (NOAA), https://www.esrl.noaa.gov/gmd/ccgg/trends/monthly.html (accessed 1 August 2020).

[2] M. E. Boot-Handford, J. C. Abanades, E. J. Anthony, M. J. Blunt, S. Brandani, N. Mac Dowell, J. R. Fernandez, M. C. Ferrari, R. Gross, J. P. Hallet, R. S. Haszeldine, P. Heptonstall, A. Lyngfelt, Z. Makuch, E. Mangano, R. T. J. Porter, M. Pourkashanian, G. T. Rochelle, N. Shah, J. G. Yao, P. S. Fenell, Carbon capture and storage update, Energ. Environ. Sci. 7 (2014) 130-189. https://doi.org/10.1039/C3EE42350F.

[3] J. Albo, T. Yoshioka, T. Tsuru, Porous Al_2O_3/TiO_2 tubes in combination with 1-ethyl-3-methylimidazolium acetate ionic liquid for CO_2/N_2 separation, Sep. Purif. Technol. 122 (2014) 440-448. https://doi.org/10.1016/j.seppur.2013.11.024.

[4] J. Albo, M. Perfecto-Irigaray, G. Beobide, A. Irabien, Cu/Bi metal-organic framework-based systems for an enhanced electrochemical transformation of CO_2 to alcohols, J. CO2 Util. 33 (2019) 157-165. https://doi.org/10.1016/j.jcou.2019.05.025.

[5] J. Albo, M. Alvarez-Guerra, P. Castaño, A. Irabien, Towards the electrochemical conversion of carbon dioxide into methanol, Green Chem. 17 (4) (2015) 2304-2324. https://doi.org/10.1039/C4GC02453B.

[6] G. Centi, E. A. Quadrelli, S. Perathoner, Catalysis for CO_2 conversion: A key technology for rapid introduction of renewable energy in the value chain of chemical industries, Energ. Environ. Sci. 6(6) (2013) 1711–1731. https://doi.org/10.1039/C3EE00056G.

[7] W. Tu, Y. Zhou, Z. Zou, Photocatalytic conversion of CO_2 into renewable hydrocarbon fuels: State-of-the-art accomplishment, challenges, and prospects, Adv. Mater. 26 (2014) 4607−4626. https://doi.org/10.1002/adma.201400087.

[8] R. Chauvy, N. Meunier, D. Thomas, G. De Weireld, Selecting emerging CO_2 utilization products for short- to mid-term deployment, Appl. Energ. 236 (2019) 662–680. https://doi.org/10.1016/j.apenergy.2018.11.096.

[9] Y. Ma, X. Wang, Y. Jia, X. Chen, H. Han, C. Li, Titanium dioxide-based nanomaterials for photocatalytic fuel generations, Chem. Rev. 114 (2014) 9987−10043. https://doi.org/10.1021/cr500008u.

[10] S. N. Habisreutinger, L. Schmidt-Mende, J. K. Stolarczyk, Photocatalytic reduction of CO_2 on TiO_2 and other semiconductors, Angew. Chem. Int. Ed. 52 (2013) 7372–7408. https://doi.org/10.1002/anie.201207199.

[11] J. Albo, Photocatalytic synthesis of methanol from CO_2 and H_2O, in: J. Albo (Ed.), Carbon Dioxide Capture: Processes, Technology and Environmental Implications, Nova Publishers, New York, 2016, pp. 277–300. ISBN: 978-163485321-7.

[12] M. Cheng, S. Yang, R. Chen, X. Zhu, Q. Liao, Y. Huang, Copper-decorated TiO_2 nanorod thin films in optofluidic planar reactors for efficient photocatalytic reduction of CO_2, Int. J. Hydrogen Energ. 42(15) (2017) 9722–9732. https://doi.org/10.1016/j.ijhydene.2017.01.126.

[13] E. Karamian, S. Sharifnia, On the general mechanism of photocatalytic reduction of CO_2, J. CO2 Util. 16 (2016) 194-203. https://doi.org/10.1016/j.jcou.2016.07.004.

[14] O. Oluwafunmilola, M. M. Maroto-Valer, Review of material design and reactor engineering on TiO_2 photocatalysis for CO_2 reduction, J. Photoch. Photobio. C. 24 (2015) 16–42. https://doi.org/10.1016/j.jphotochemrev.2015.06.001.

[15] N. Wang, X. Zhang, Y. Wang, W. Yu, H. L. W. Chan, Microfluidic reactors for photocatalytic water purification, Lab. Chip. 14 (2014) 1074–1082. https://doi.org/10.1039/C3LC51233A.

[16] L. Li, R. Chen, Q. Liao, X. Zhu, G.Y. Wang, D.Y. Wang, High surface area optofluidic microreactor for redox mediated photocatalytic water splitting, Int. J. Hydrogen Energ. 39 (2014) 19270–19276. https://doi.org/10.1016/j.ijhydene.2014.05.098.

[17] L. Li, R. Chen, X. Zhu, H. Wang, Y.Z. Wang, Q. Liao, D.Y. Wang, Optofluidic microreactors with TiO_2-coated fiber glass, ACS Appl. Mater. Inter. 5 (2013) 12548–12553. https://doi.org/10.1021/am403842b.

[18] M. Cheng, Y. Huang, R. Gao, S. Bai1, Numerical simulation of photocatalytic reduction of gas phase CO2 in optofluidic microreactor, Catal. Lett. 149 (2019) 3000–3011. https://doi.org/10.1007/s10562-019-02838-z.

[19] X. Cheng, R. Cheng, X. Zhu, Q. Liao, L. An, D. Ye, X. He, S. Li, An optofluidic planar microreactor for photocatalytic reduction of CO_2 in alkaline environment, Energy. 120 (2017) 267–282. https://doi.org/10.1016/j.energy.2016.11.081.

[20] R. Chen, X. Cheng, X. Zhu, Q. Liao, L. An, D. Ye, X. He, Z. Wang, High-performance optofluidic membrane microreactor with a mesoporous CdS/TiO_2/SBA-15@carbon paper composite membrane for the CO_2 photoreduction, Chem. Eng. J. 316 (2017) 911–918. https://doi.org/10.1016/j.cej.2017.02.044.

[21] X. Cheng, R. Chen, X. Zhu, Q. Liao, X. He, S. Li, L. Li, Optofluidic membrane microreactor for photocatalytic reduction of CO_2, Int. J. Hydrogen Energ. 41 (2016) 2457–2465. https://doi.org/10.1016/j.ijhydene.2015.12.066.

[22] J. Dupont, J. D. Scholtena, On the structural and surface properties of transition-metal nanoparticles in ionic liquids, Chem. Soc. Rev. 39 (2010) 1780-1804. https://doi.org/10.1039/B822551F.

[23] L. P. Matte, A. S. Kilian, L. Luza, M. C. M. Alves, J. Morais, D. L. Baptista, J. Dupont, F. Bernardi, Influence of the CeO_2 support on the reduction properties of Cu/CeO_2 and Ni/CeO_2 nanoparticles, J. Phys. Chem. C. 119(47) (2015) 26459–26470. https://doi.org/10.1021/acs.jpcc.5b07654.

[24] J. Albo, A. Irabien, Cu_2O-loaded gas diffusion electrodes for the continuous electrochemical reduction of CO_2 to methanol, J. Catal. 343 (2016) 232–239. https://doi.org/10.1016/j.jcat.2015.11.014.

[25] H. Cheng, J. Wang, Y. Zhao, X. Han, Effect of phase composition, morphology, and specific surface area on the photocatalytic activity of TiO_2 nanomaterials, RSC Adv. 4 (2014) 47031-47038. https://doi.org/10.1039/C4RA05509H.

[26] E. Silva Junior, F. A. La Porta, M. S. Liu, J. Andrés, J. A. Varela, E. Longo. A relationship between structural and electronic order–disorder effects and optical properties in crystalline TiO_2 nanomaterials. Dalton Trans. 44 (2015) 3159-3175. https://doi.org/10.1039/C4DT03254C.

[27] M. C. Biesinger. Advanced analysis of copper X-ray photoelectron spectra. Surf. Interface Anal. 49 (2017) 1325–1334. https://doi.org/10.1002/sia.6239.

[28] C. Valdebenito, J. Pinto, M. Nazarkovsky, G. Chacón, O. Martínez-Ferraté, K. Wrighton-Araneda, D. Cortés-Arriagada, M. B. Camarada, J. A. Fernandes, G. Abarca, Highly modulated supported triazolium-based ionic liquids: direct control of the electronic environment on Cu nanoparticles, Nanoscale Adv. 2 (2020) 1325-1332. https://doi.org/10.1039/D0NA00055H.

[29] K. C. Christoforidis, M. Fernandez-Garcia, Photoactivity and charge trapping sites in copper and vanadium doped anatase TiO_2 nano-materials, Catal. Sci. Technol. 6 (2016) 1094-105. https://doi.org/10.1039/C5CY00929D.

[30] N. C.T. Martinsa, J. Ângeloa, A. V. Girãob, T. Trindadeb, L. Andradea, A. Mendesa, N-doped carbon quantum dots/TiO_2 composite with improved photocatalytic activity, Appl. Catal B-Environ. 193 (2016) 67–74. http://dx.doi.org/10.1016/j.apcatb.2016.04.016.

[31] J. O. Olowoyo, M. Kumar, T. Dash, S. Saran, S. Bhandari, U. Kumar, Self-organized copper impregnation and doping in TiO_2 with enhanced photocatalytic conversion of H_2O and CO_2 to

fuel, Int. J. Hydrogen Energ. 43 (2018) 19468–19480. https://doi.org/10.1016/j.ijhydene.2018.08.209.

[32] I.-H. Tseng, J. C.S. Wu, H.-Y. Chou, Effects of sol–gel procedures on the photocatalysis of Cu/TiO_2 in CO_2 photoreduction, J. Catal. 221 (2004) 432–440. https://doi.org/10.1016/j.jcat.2003.09.002.

[33] M. Hussain, P. Akhter, G. Saracco, N. Russo, Nanostructured TiO_2/KIT-6 catalysts for improved photocatalytic reduction of CO_2 to tunable energy products, Appl. Catal. B-Environ. 170-171 (2015) 53-65. https://doi.org/10.1016/j.apcatb.2015.01.007.

[34] Patsoura, D.I. Kondarides, X.E. Verykios, Photocatalytic degradation of organic pollutants with simultaneous production of hydrogen, Catal. Today. 124 (2007) 94–102. https://doi.org/10.1016/j.cattod.2007.03.028.

[35] K. C. Christoforidis, P. Fornasiero, Photocatalysis for Hydrogen Production and CO_2 Reduction: The Case of Copper-Catalysts, ChemCatChem, 9 (2019) 368-382. https://doi.org/10.1002/cctc.201801198.

[36] J. Albo, D. Vallejo, G. Beobide, O. Castillo, P. Castaño, A. Irabien, Copper-based Metal–Organic Porous Materials for CO_2 electrocatalytic reduction to alcohols, ChemSusChem. 10 (2017) 1100-1109. https://doi.org/10.1002/cssc.201600693.

[37] Q. Luo, Y. Cao, Z. Liu, B. Feng, Q. Zhou, N. Li, A feasible process for removal and utilization of CO_2 in thermal power plants by MDEA+DMSO scrubbing and Cu/TiO_2 photocatalytic reduction, Appl. Therm. Eng. 153 (2019) 369–378. https://doi.org/10.1016/j.applthermaleng.2019.02.049.

[38] Y. N. Kavil, Y. A. Shaban, R. K. Al Farawati, M. I. Orif, M. Zobidi, S. U. M. Khan, Efficient photocatalytic reduction of CO_2 present in seawater into methanol over Cu/C-Co-doped TiO_2 nanocatalyst under UV and natural sunlight, Water Air Soil Pollut. (2018) 229-236. https://doi.org/10.1007/s11270-018-3881-3.

[39] Y. N. Kavil, Y. A. Shaban, R. K. Al Farawati, M. I. Orif, M. Zobidi, S. U.M. Khan, Photocatalytic conversion of CO_2 into methanol over Cu-C/TiO_2 nanoparticles under UV light and natural sunlight, J. Photoch. Photobio. A., 347 (2017) 244–253. https://doi.org/10.1016/j.jphotochem.2017.07.046.

[40] H. Li, C. Li, L. Han, C. Li, S. Zhang, Photocatalytic reduction of CO_2 with H_2O on CuO/TiO_2 catalysts, Energ. Source Part A. 38(3) (2016) 420-426. https://doi.org/10.1080/15567036.2011.598910.

[41] H.-C. Yang, H.-Y. Lin, Y.-S. Chien, J. C.-S. Wu, H.-H. Wu, Mesoporous TiO_2/SBA-15, and Cu/TiO_2/SBA-15 composite photocatalysts for photoreduction of CO_2 to methanol, Catal Lett. 131 (2009) 381–387. https://doi.org/10.1007/s10562-009-0076-y.

[42] Slamet, H.W. Nasution, E. Purnama, K. Riyani, J. Gunlazuardi, Effect of copper species in a photocatalytic synthesis of methanol from carbon dioxide over copper-doped titania catalysts, World Applied Sciences Journal 6 (1) (2009) 112-122. ISSN 1818-4952.

[43] Slamet, H. W. Nasution, E. Purnama, S. Kosela, J. Gunlazuardi, Photocatalytic reduction of CO_2 on copper-doped titania catalysts prepared by improved-impregnation method, Catal. Commun. 6(5) (2005) 313–319. https://doi.org/10.1016/j.catcom.2005.01.011.

[44] I.-H. Tseng, J. C.-S. Wu, Chemical states of metal-loaded titania in the photoreduction of CO_2, Catal. Today. 97 (2004) 113–119. https://doi.org/10.1016/j.cattod.2004.03.063.

[45] I.-H. Tseng, W-C. Chang, J. C. S. Wu, Photoreduction of CO_2 using sol–gel derived titania and titania-supported copper catalysts, Appl. Catal. B-Environ. 37 (1) (2002) 37-48. https://doi.org/10.1016/S0926-3373(01)00322-8.

[46] B. Li, W. Niu, Y. Cheng, J. Gu, P. Ning, Q. Guan, Preparation of Cu_2O modified TiO_2 nanopowder and its application to the visible light photoelectrocatalytic reduction of CO_2 to CH_3OH. Chem, Phys. Lett. 700 (2018) 57-63. https://doi.org/10.1016/j.cplett.2018.03.049.

[47] E. Liu, L. Qi, J. Bian, Y. Chen, X. Hu, J. Fan, H. Liu, C. Zhu, Q. Wang, A facile strategy to fabricate plasmonic Cu modified TiO_2 nano-flower films for photocatalytic reduction of CO_2 to methanol, Mater. Res. Bull. 68 (2015) 203–209. https://doi.org/10.1016/j.materresbull.2015.03.064.

[48] L. Liu, W. Yang, Q. Li, S. Gao, J. K. Shang, Synthesis of Cu_2O nanospheres decorated with TiO_2 nanoislands, their enhanced photoactivity and stability under visible light illumination, and their post-illumination catalytic memory, ACS Appl. Mater. Inter. 6 (8) (2015) 5629-5639. https://doi.org/10.1021/am500131b.

[49] J. Wang, G. Ji, Y. Liu, M.A. Gondal, X. Chang, Cu_2O/TiO_2 heterostructure nanotube arrays prepared by an electrodeposition method exhibiting enhanced photocatalytic activity for CO_2 reduction to methanol, Catal. Commun. 46 (2014) 17-21. https://doi.org/10.1016/j.catcom.2013.11.011.

[50] A. E. Nogueira, J. A. Oliveira, G. T. S. T. da Silva, C. Ribeiro. Insights into the role of CuO in the CO_2 photoreduction process. Sci. Rep. 9 (2019) 1316. https://doi.org/10.1038/s41598-018-36683-8.

[51] F. Xu, J. Zhang, B. Zhu, J. Yu, J. Xu, $CuInS_2$ sensitized TiO_2 hybrid nanofibers for improved photocatalytic CO_2 reduction, Appl. Catal. B-Environ. 230 (2018) 194-202. https://doi.org/10.1016/j.apcatb.2018.02.042.

[52] Z. Q. He, L. X. Jiang, J. Han, L. N. Wen, J. M. Chen, S. Song, Activity and selectivity of Cu and Ni doped TiO_2 in the photocatalytic reduction of CO_2 with H_2O under UV-light irradiation, Asian J. Chem. 26 (15) (2014) 4759-4766. https://doi.org/10.14233/ajchem.2014.16199.

[53] T. Yang, Q. Yu, H. Wang, Photocatalytic Reduction of CO_2 to CH_3OH coupling with the oxidation of amine to imine, Catal. Lett. 148 (2018) 2382–2390. https://doi.org/10.1007/s10562-018-2412-6.

[54] M. R. Uddin, M. R. Khan, M. W. Rahman, A. Yousuf, C. K. Cheng, Photocatalytic reduction of CO_2 into methanol over $CuFe_2O_4/TiO_2$ under visible light irradiation, Reac. Kinet. Mech. Cat. 116 (2015) 589–604. https://doi.org/10.1007/s11144-015-0911-7.

[55] J. C.S. Wu, H.-M. Lin, C.-L. Lai, Photo reduction of CO_2 to methanol using optical-fiber photoreactor, Appl. Catal. A-Gen. 296 (2005) 194–200. https://doi.org/10.1016/j.apcata.2005.08.021.

[56] K. Hirano, K. Inoue, T. Yatsu, Photocatalysed reduction of CO_2 in aqueous TiO_2 suspension mixed with copper powder, J. Photochern. Photobiol. A: Chem. 64 (1992) 255-258. https://doi.org/10.1016/1010-6030(92)85112-8.

[57] S. Nadeem, A. Mumtaz, M. Mumtaz, M. I. A. Mutalib, M. S. Shaharun, B. Abdullah, Visible light driven CO_2 reduction to methanol by Cu-porphyrin impregnated mesoporous Ti-MCM-48, J. Mol. Liq. 272 (2018) 656–667. https://doi.org/10.1016/j.molliq.2018.09.077.

[58] D. O. Adekoya, M. Tahir, N. A. S. Amin, g-C_3N_4/(Cu/TiO_2) nanocomposite for enhanced photoreduction of CO_2 to CH_3OH and HCOOH under UV/visible light, J. CO2 Util. 18 (2017) 261–274. https://doi.org/10.1016/j.jcou.2017.02.004.

[59] M. Tahir, B. Tahir, N. A. S. Amina, H. Alias, Selective photocatalytic reduction of CO_2 by H_2O/H_2 to CH_4 and CH_3OH over Cu-promoted In_2O_3/TiO_2 nanocatalyst, Appl. Surf. Sci. 389 (2016) 46–55. https://doi.org/10.1016/j.apsusc.2016.06.155.

[60] M. M. R. Khan, M. R. Uddin, H. Abdullah, K. M. R. Karim, A. Yousuf, C. K. Cheng, H. R. Ong, Preparation and characterization of $CuFe_2O_4/TiO_2$ photocatalyst for the conversion of CO_2 into methanol under visible light, International Journal of Chemical and Molecular Engineering. 10 (2016). https://doi.org/10.10.5281/zenodo.1126852.

[61] Y.-H. Cheng, V.-H. Nguyen, H.-Y. Chan, J. C.S. Wu, W.-H. Wang, Photo-enhanced hydrogenation of CO_2 to mimic photosynthesis by CO co-feed in a novel twin reactor, Appl. Energ. 147 (2015) 318–324. https://doi.org/10.1016/j.apenergy.2015.02.085.

[62] J.-J. Wang, Y.-H. Jing, T. Ouyang, Q. Zhang, C.-T. Chang, Photocatalytic reduction of CO_2 to energy products using Cu–TiO_2/ZSM-5 and Co–TiO_2/ZSM-5 under low energy irradiation, Catal. Commun. 59 (2015) 69-72. https://doi.org/10.1016/j.catcom.2014.09.030.

[63] O. Oluwafunmilola, M. M. Maroto-Valera, Copper based TiO_2 honeycomb monoliths for CO_2 photoreduction, Catal. Sci. Technol. 4 (2014) 1631–1637. https://doi.org/10.1039/C3CY00991B.

[64] M. Bellardita, A. Di Paola, E. García-López, V. Loddo, G. Marcì, L. Palmisano, Photocatalytic CO_2 reduction in gas-solid regime in the presence of bare, SiO_2 supported or Cu-loaded TiO_2 samples, Curr. Org. Chem. 17 (2013) 2440-2448. https://doi.org/10.2174/13852728113179990057.

[65] B. Srinivas, B. Shubhamangala, K. Lalitha, P. A. K. Reddy, V. D. Kumari, M. Subrahmanyam, B. R. De, Photocatalytic reduction of CO_2 over Cu-TiO_2/molecular sieve 5A composite. Photochem. Photobiol. 87 (2011) 995-1001. https://doi.org/10.1111/j.1751-1097.2011.00946.x.

[66] D. Luo, Y. Bi, W. Kan, N. Zhang, S. Hong, Copper and cerium co-doped titanium dioxide on catalytic photo reduction of carbon dioxide with water: Experimental and theoretical studies, J. Mol. Struct. 994 (2011) 325-331. https://doi.org/10.1016/j.molstruc.2011.03.044.

[67] J. C. S. Wu, H.-M. Lin, Photo reduction of CO_2 to methanol via TiO_2 photocatalyst, Int. J. Photoenergy. (2005) 115-119. https://doi.org/10.1155/S1110662X05000176.

[68] G. Guan, T. Kida, A. Yoshida, Reduction of carbon dioxide with water under concentrated sunlight using photocatalyst combined with Fe-based catalyst, Appl. Catal. B-Environ. 41 (2003) 387–396. https://doi.org/10.1016/S0926-3373(02)00174-1.

[69] M. Anpo, H. Yamashita, Y. Ichihashi, S. Ehara, Photocatalytic reduction of CO_2 with H_2O on various titanium oxide catalysts, J. Electroanal. Chem. 396 (1995) 21-26. https://doi.org/10.1016/0022-0728(95)04141-A.

[70] H. Yamashita, H. Nishiguchi, N. Kamada, M. Anpo, Y. Teraoka, H. Hatano, S. Ehara, K. Kikui, L. Palmisano, A. Sclafani, M. Schiavello, M. A. Fox, Photocatalytic reduction of CO_2 with H_2O on TiO_2 and Cu/TiO_2 catalysts, Res. Chem. Intermed. 20 (8) (1994) 815-823. https://doi.org/10.1007/s11356-017-0944-8.

Declaration of interests

☒ The authors declare that they have no known competing financial interests or personal relationships that could have appeared to influence the work reported in this paper.

☐The authors declare the following financial interests/personal relationships which may be considered as potential competing interests:

2020.8.6

Highlights

- An optofluidic microreactor is used for continuous photoreduction of CO_2 to CH_3OH
- Cu NPs are synthesized in ionic liquid and embedded in TiO_2 as photocatalysts
- Reaction yield is determined by Cu content, catalyst loading and light intensity
- In a two-compartment configuration, CH_3OH formation declines in favour of C_2H_5OH
- The system outperforms Cu/TiO_2-based systems for CO_2 phororeduction to CH_3OH